Plasma Science and Technology

PAPER

Enhancing toluene removal in a plasma photocatalytic system through a black TiO_2 photocatalyst

Plasma Sci. Technol. **21** (2019) 115503 (9pp) https://doi.org/10.1088/2058-6272/ab3668

Enhancing toluene removal in a plasma photocatalytic system through a black TiO_2 photocatalyst

Bin ZHU (朱斌)[1], **Luyao ZHANG** (张璐瑶), **Yan YAN** (闫妍), **Meng LI** (李猛) **and Yimin ZHU** (朱益民)[1]

Collaborative Innovation Center for Vessel Pollution Monitoring and Control, Dalian Maritime University, Dalian 116026, People's Republic of China

E-mail: binzhu@dlmu.edu.cn and ntp@dlmu.edu.cn

Received 8 May 2019, revised 29 July 2019
Accepted for publication 29 July 2019
Published 5 September 2019

Abstract

An efficient toluene removal in air using a plasma photocatalytic system (PPS) not only needs favorable surface reactions over photocatalysts under the action of plasma, but also requires the photocatalysts to efficiently absorb light emitted from the discharge for driving the photocatalytic reactions. We report here that the PPS constructed by integrating a black titania (B-TiO_2) photocatalyst with a dielectric barrier discharge (DBD) can effectively remove toluene with above 70% CO_2 selectivity and remarkably reduced the concentration of secondary pollutants of ozone and nitrogen oxides at a specific energy input of 1500 $J \cdot l^{-1}$, while exhibiting good stability. Photocatalyst characterizations suggest that the B-TiO_2 provides a high concentration of oxygen vacancies for the surface oxidation of toluene in DBD, and efficiently absorbs ultraviolet–visible light emitted from the discharge to induce plasma photocatalytic oxidation of toluene. The presence of B-TiO_2 in the plasma region also results in a high discharge efficiency, facilitating the generation of large numbers of reactive species and thus the oxidation of toluene towards CO_2. The greatly enhanced performance of the PPS integrated with B-TiO_2 in toluene removal offers a promising approach to efficiently remove refractory volatile organic compounds from air at low temperatures.

Keywords: plasma photocatalysis, black TiO_2, synergetic effect, dielectric barrier discharge, toluene removal

(Some figures may appear in colour only in the online journal)

1. Introduction

Plasma catalysis is a promising technique, which is commonly constructed by *in situ* integration of non-thermal plasma and catalysts, exhibiting extensive applications in material modification, fuel reforming and environmental pollution control [1–3]. In particular, many efforts in plasma catalysis have been devoted to the abatement of volatile organic compounds (VOCs) because the plasma catalytic system (PCS) possesses advantages of high energy efficiency, low operating temperature, fast mineralization rate and low by-product formation for removing the refractory VOCs [4–6]. Recently, the combination of non-thermal plasma and photocatalysts (plasma photocatalysis) has attracted increasing attention in the field of VOC removal, since the plasma photocatalytic system (PPS) can utilize light emitted from the discharge to drive a series of photoreactions in comparison with the conventional PCS [7–9].

Photocatalysts in the PPS show significant influence on the performance of VOC removal, since they contribute to the activity of the PPS and also largely determine the distribution of products. Currently, titania (TiO_2) is the most-used photocatalyst due to its low cost, nontoxicity and superior stability [10, 11]. Nevertheless, owing to its wide band gap (>3.0 eV), the conventional TiO_2 only exhibits ultraviolet (UV) photocatalytic

[1] Authors to whom any correspondence should be addressed.

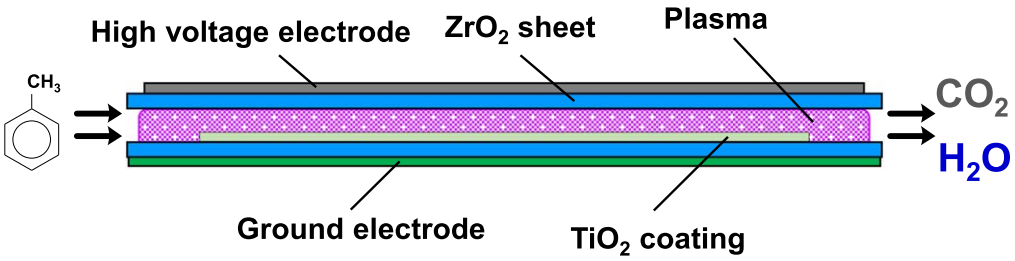

Figure 1. Configuration of the PPS for toluene removal.

activity, which limits the utilization of visible light emitted from the discharge. Black TiO_2 (B-TiO_2) is regarded as a potential candidate to extend the light absorption of TiO_2 to the visible region. In general, B-TiO_2 with a narrow band gap (~1.5 eV) is characterized by a high concentration of oxygen vacancies, leading to its unique crystal and electronic structures as well as its surface property, and thus entire/part absorption for visible light [12, 13]. Integrating B-TiO_2 with non-thermal plasma would bring triple advantages to the removal of VOCs. Firstly, the abundant oxygen vacancies of B-TiO_2 facilitate the surface reactions between absorbed VOC molecules and reactive species formed in plasma, resulting in a strong synergetic effect between B-TiO_2 and the discharge. Secondly, B-TiO_2 can simultaneously absorb UV and visible light emitted from the discharge to effectively induce the photocatalytic oxidation of VOCs. Lastly, reactive species (energetic electrons, oxygen atoms, etc) generated by non-thermal discharge can also degrade VOC molecules via the gas-phase reactions. Thereby, a PPS consisting of non-thermal plasma and B-TiO_2 is expected to be a highly efficient approach for the purification of refractory VOCs.

In this work, we constructed a PPS by combining a dielectric barrier discharge (DBD) with a B-TiO_2 photocatalyst for the first time for the purpose of efficiently removing the typical aromatic VOC-toluene. To make the photocatalysts fully interact with the plasma in toluene removal, coated samples were prepared by coating photocatalysts on a glass substrate and were placed within a flat plate DBD reactor. It was found that, for toluene removal in PPS, the B-TiO_2 can achieve much higher toluene conversion and CO_2 selectivity, as well as lower secondary pollutants, than the conventional TiO_2 photocatalyst under the same conditions. The effect of photocatalysts on discharge characteristics was investigated. Further, the photocatalysts were characterized by x-ray diffraction (XRD), Raman spectra, UV–vis diffuse reflectance spectra (UV–vis DRS) and photoluminescence (PL) spectra methods to unravel their distinct performance in the plasma photocatalytic processes. This study would provide a novel perspective for the plasma photocatalysis technique to efficiently remove the refractory VOCs.

2. Experimental

2.1. Preparation of photocatalysts

The conventional TiO_2 (P25, Degussa) and B-TiO_2 (Shanghai Institute of Ceramics, China) were used as photocatalysts to construct the PPS, respectively. To prepare the photocatalyst's coating (as mentioned in the introduction), about 35 mg sample was coated on a glass substrate of 75 mm (length) × 25 mm (width) × 1 mm (thickness) using a drip-coating method and dried at 80 °C for 1 h [11, 14]. The weight of the coated sample was controlled within 35 ± 1 mg. In this study, the PPS integrated with P25 and B-TiO_2 photocatalysts were denoted as PPS (P25) and PPS (B-TiO_2), respectively.

2.2. Plasma photocatalytic removal of toluene

Plasma photocatalytic removal of toluene was performed in a home-made flat plate DBD reactor, and the configuration of the reactor is shown in figure 1. Briefly, two ZrO_2 ceramic sheets with thickness of 0.25 mm were used as a double dielectric barrier between the high voltage and ground electrodes. A stainless steel mesh of 80 mm (length) × 25 mm (width) covering the upper ZrO_2 sheet and a silver coating of 90 mm (length) × 25 mm (width) on the under sheet were used as the high voltage electrode and ground electrode, respectively. The discharge gap of the DBD reactor is 2 mm. In the toluene removal process, the photocatalyst coating was placed within the discharge region, and a 1.8 kHz AC power source (CTP-2000K, Nanjing Suman Electronics Co., Ltd, China) was applied to the DBD reactor. The toluene removal experiments were conducted according to the following sequence. First, the PPS (discharge off) was first purged with 200 ml min^{-1} N_2 for 30 min. Then, synthetic air (80% N_2 + 20% O_2) containing ~100 ppm toluene with a flow rate of 200 ml min^{-1} was switched into the PPS (discharge on) for toluene removal. After the toluene removal, N_2 (200 ml min^{-1}) was switched into the PPS (discharge off) again to purge the reactor for 30 min. The products from the PPS were analyzed online with a gas chromatograph (GC, Tianmei 7900, China), an ozone analyzer (Mini-Hicon, USA) and a Fourier-transform infrared (FT-IR) spectrometer (IGS, Thermofisher, USA), respectively. The intermediate products during the toluene removal process were also evaluated by a mass spectrometer (HPR 20 QIC, HIDEN Analytical, United Kingdom). For comparison, photocatalytic performance of the photocatalysts in toluene removal was investigated in a single-pass continuous-flow photocatalytic oxidation reactor [11, 15]. A xenon lamp (within 300–800 nm range) located at the top of the quartz window of the photocatalytic oxidation reactor was used as the light source [16], and the light intensity on the surface of the photocatalysts was measured by an optical power and energy meter (PM100USB, Thorlabs, USA) [11].

Toluene conversion ($X_{C_7H_8}$) and CO_2 selectivity (S_{CO_2}) were calculated by the following two equations.

$$X_{C_7H_8} = \frac{(C_{in} - C_{out})}{C_{in}} \quad (1)$$

$$S_{CO_2} = \frac{C_{CO_2}}{7 \cdot (C_{in} - C_{out})} \quad (2)$$

where C_{in} and C_{out} are the inlet and outlet concentrations of toluene, respectively; C_{CO_2} denotes the outlet concentration of CO_2.

The emission spectra of the discharge within the range of 200–800 nm were recorded using a spectrometer (INS-300-122B, Acton, USA). An oscilloscope (DPO4108B, Tektronix) equipped with a high voltage probe (P6015A, Tektronix), current probe (P2220, Tektronix), sampling resistance (51 Ω) and capacitor (0.47 μF) was used to monitor the waveforms of the voltage and current as well as Lissajous figures. Input power (P_{in}) was measured with a wattmeter installed in the primary side of the transformer, and the specific energy input (SEI) ($J \cdot l^{-1}$) and energy efficiency (EE) of the removal reaction was calculated by equations (3) and (4) [17]:

$$SEI = \frac{P_{in}}{F_{in}} \quad (3)$$

$$EE = \frac{3.6 \cdot C_{in} \cdot X_{C_7H_8} \cdot M}{SEI \cdot V_M} \quad (4)$$

where F_{in} represents the total flow rate of reactant gas; M and V_M denote the molar mass of toluene (g mol^{-1}) and the molar volume of gas (l mol^{-1}) under the ambient condition (298 K), respectively.

2.3. Photocatalyst characterization

The phase compositions of the photocatalysts were investigated by XRD analysis on a PANalytical Empyrean diffractometer equipped with a Cu Kα radiation source ($\lambda = 1.5418$ Å) operating at 40 mA and 40 kV.

UV–vis DRS of the photocatalysts were performed using a lambda 750 s spectrometer (Perkin-Elmer, USA) within the wavelength range of 200–800 nm. Before the measurement of the photocatalysts, barium sulfate was first tested to use as a background reference.

A fluorescence spectrometer (F-700, Hitachi, Japan) with a light source of a 150 W xenon lamp and an excitation wavelength of 300 nm was applied to testing the PL spectra of the photocatalysts. The scanning range and speed were set as 240 nm min^{-1} and 320–580 nm, respectively.

Raman spectra measurements were performed on a LabRAM HR 800 Raman spectrometer using a 532 nm (He-Ne laser) laser as the excitation source. The laser power on the samples was 0.8 mW. Each sample was scanned at least three times to obtain reliable spectra.

3. Results and discussion

3.1. Discharge characteristics

The discharge voltage and current, Lissajous figures and typical emission spectrum in toluene removal processes are shown in figure 2. From figures 2(a) and (b), numerous current pulses of microdischarge are observed for both the DBD alone and the PPS (B-TiO_2), demonstrating a typical filamentary DBD mode of the discharges [18, 19]. Compared with the DBD alone, the presence of the B-TiO_2 coating in the PPS leads to a decrease in discharge voltage and an obvious increase in current amplitude at the same P_{in}. This might be attributed to the reduction in the discharge gap (d_g) with loading the B-TiO_2 coating into the discharge region. According to equation (5), the capacitance of the dielectric (C_d) of the DBD reactor would increase with the decrease in d_g, which results in the decrease in the discharge voltage and increase in discharge current at the same P_{in} [20, 21]. This point is also supported by the Lissajous figures. As shown in figure 2(c), the PPS (B-TiO_2) presents a similar Lissajous figure of a parallelogram to that of the DBD alone, but it possesses a lower discharge voltage and a much larger amount of transferred charge at the same P_{in} owing to the reduced C_d values (the slope of the dotted line in figure 2(c)). Moreover, the inset of figure 2(c) also indicates that the presence of B-TiO_2 in the PPS causes an enhancement in the discharge power (0.85 W) compared with the DBD alone (0.51 W). All the above results, taken together, suggest that the B-TiO_2 coating located in the discharge region makes the PPS obtain higher plasma density and discharge efficiency than the DBD alone at the same P_{in}, facilitating the generation of large numbers of reactive species, strong interaction between plasma and B-TiO_2 and thus toluene removal. Note that the PPS (P25) exhibits similar electric discharge characteristics to those of the PPS (B-TiO_2), indicating that the properties of photocatalysts show a weak influence on the discharge during the toluene removal process.

$$C_d = \varepsilon S / d_g \quad (5)$$

where ε and S represent the dielectric constant and plasma area, respectively.

The light emitted from the discharge provides the driven force for the photocatalytic oxidation of toluene over photocatalysts. Figure 2(d) shows the typical emission spectrum collected from the PPS (B-TiO_2) during the toluene removal. Owing to the synthetic air composition of the discharge gas, a series of characteristic emission lines, such as N_2 second positive ($C^3\Pi_u \rightarrow B^3\Pi_g$, 300–450 nm), N_2 ($4d^4P \rightarrow 3p^4P^0$, 673.82 nm) and O ($3p^5P \rightarrow 3s^5S_2{}^0$, 777.41 nm), can be detected. Further, NO_γ and NO_β ($B^2\Pi \rightarrow X^2\Pi$) in the range of 200–290 nm are also observed because of the reactions between O_2 and N_2 in the discharge. This indicates that the PPS (B-TiO_2) emits UV and visible light simultaneously, suggesting that greatly enhancing the performance of the PPS in toluene removal could be available if the photocatalysts can efficiently utilize the full spectrum light to induce toluene oxidation reactions.

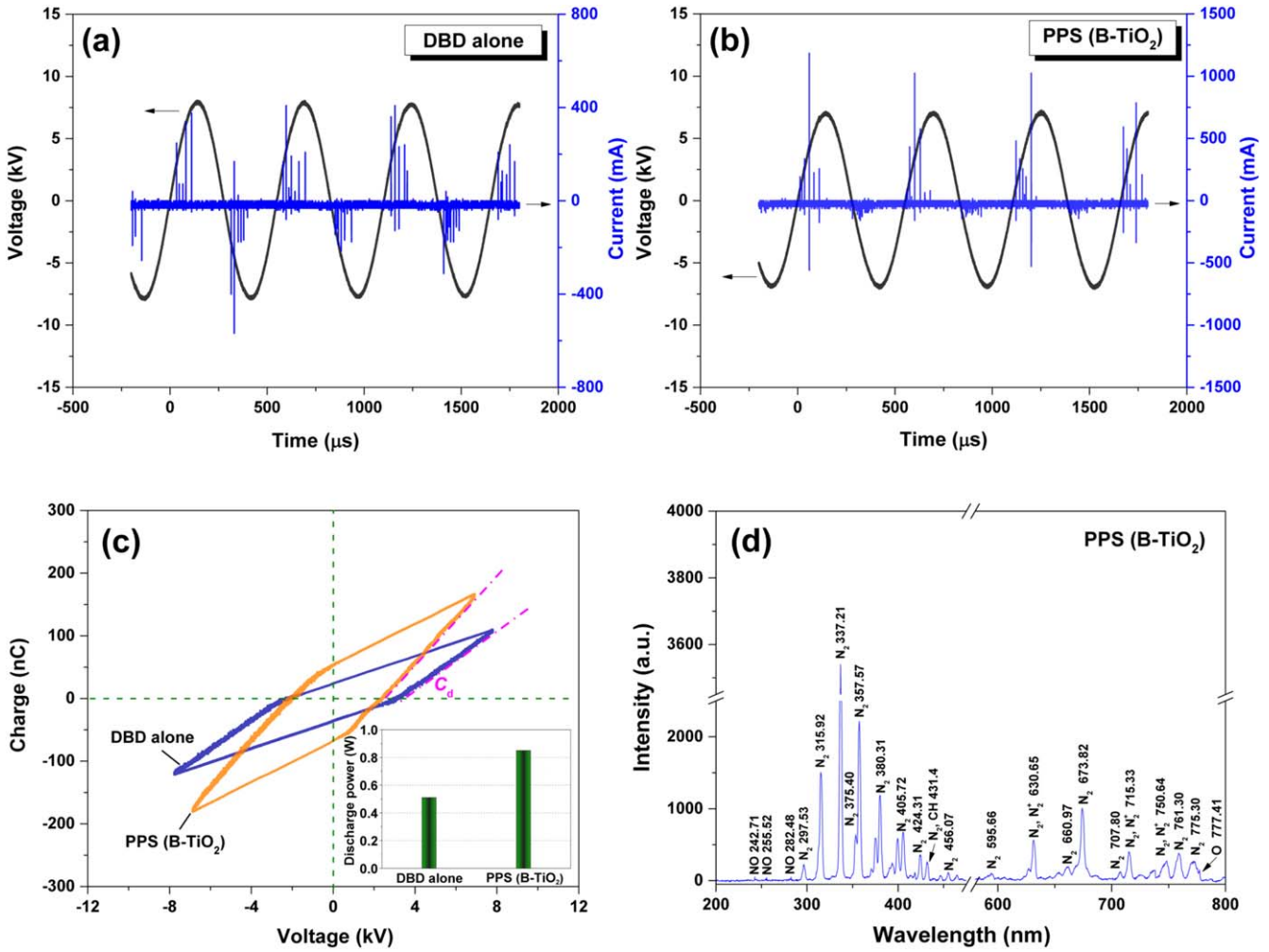

Figure 2. Waveforms of the discharge voltage and current of the DBD alone (a), PPS (B-TiO_2) (b), and their Lissajous figures (c) and a typical emission spectrum (d) in the toluene removal process. Inset of (c): discharge power for DBD alone and PPS (B-TiO_2) at P_{in} of 5 W.

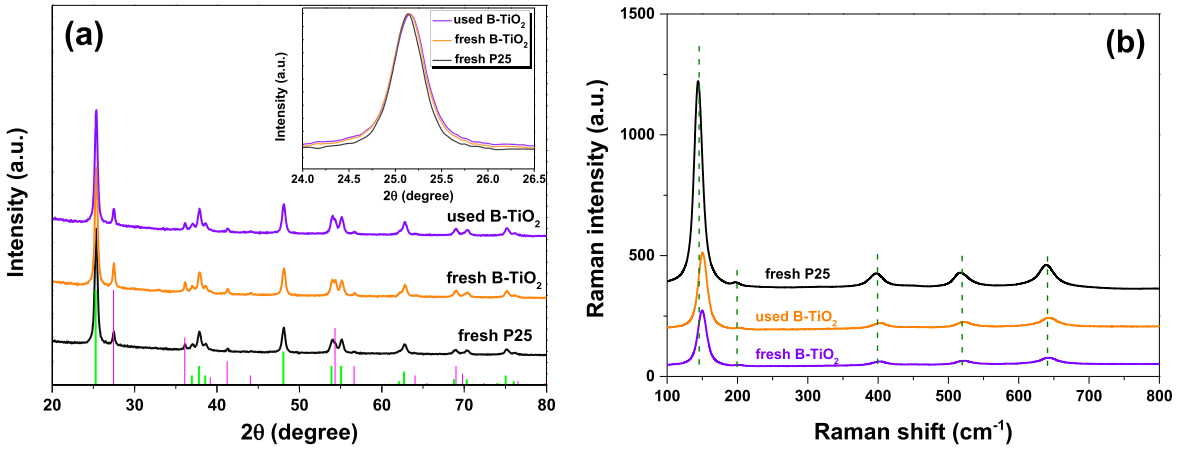

Figure 3. XRD patterns (a) and Raman spectra (b) of the photocatalysts. Inset of (a): enlarged diffraction peaks. The used B-TiO_2 was obtained after a cycled toluene removal reaction at an SEI of 1500 $J \cdot l^{-1}$; two cycles were respectively performed for 15 h with an interval of 9 h.

3.2. Physicochemical properties of the photocatalysts

3.2.1. Structural features of the photocatalysts. In figure 3(a), XRD patterns of fresh P25, fresh and used B-TiO_2 are all illustrated. Obviously, both P25 and B-TiO_2 present as a mixture of anatase and rutile. The diffraction peaks of the anatase phase at $2\theta = 25.3°$, 37.8°, 48.1°, 62.7° and 75.1°, and the rutile phase at $2\theta = 27.5°$, 36.1°, 41.2°, 54.4° and 69.1° can be clearly observed from figure 3(a). Notably, the

Table 1. Data of the characteristic band in the Raman spectra for the photocatalysts.

Photocatalyst	Position of characteristic band (cm^{-1})	FWHM (cm^{-1})
Fresh P25	144	16.2
Fresh B-TiO_2	150	20.1
Used B-TiO_2	150	19.1

Note: data of the Raman mode (E_g) with frequency at around 144 cm^{-1} is summarized; E_g represents the Raman active mode of anatase in the photocatalysts.

inset of figure 3(a) shows that B-TiO_2 exhibits a larger linewidth than P25, suggesting the higher concentration of oxygen vacancies and reduced crystal size of B-TiO_2 [22]. In addition, to investigate the durability of B-TiO_2 in plasma photocatalytic removal of toluene, we also measured the XRD pattern of the used B-TiO_2. As shown in figure 3(a), no obvious change in the diffraction pattern of B-TiO_2 occurred, even after 30 h toluene removal reaction, indicating a relative stability of B-TiO_2 in the plasma photocatalytic process. The structural properties of photocatalysts were also tested by the Raman spectrum. Figure 3(b) shows that both P25 and B-TiO_2 appear as Raman active modes with frequencies at 144, 197, 399, 515 and 639 cm^{-1}, which are assigned to the vibration of the anatase phase [13, 23]. The intensities of characteristic peaks for the fresh and used B-TiO_2 show a decline compared with the fresh P25, which is probably attributed to the absorption of the excitation laser and scattering light by B-TiO_2. Further, according to the data summarized in table 1, typical characteristic peaks of the fresh and used B-TiO_2 not only possess larger full width at half maximum (FWHM) but also exhibit a positive shift compared with P25. This suggests a much higher content of oxygen vacancies existing in B-TiO_2 [13, 23], which is consistent with the XRD results. For the toluene removal in the PPS (B-TiO_2), a high content of oxygen vacancies in B-TiO_2 means the favorable surface oxidation reactions under the plasma action, thus benefiting the conversion of toluene towards CO_2.

3.2.2. Optical properties of the photocatalysts. Considering the important role of photocatalytic reactions in toluene removal, the photoresponse of the photocatalysts was evaluated by UV–vis DRS measurement. Figure 4(a) shows that both P25 and B-TiO_2 appear to have strong absorption for UV light (<400 nm). Moreover, B-TiO_2 even exhibits strong absorption for light with a wavelength larger than 400 nm, indicating its strong absorption ability for both UV and visible light. The color of the coated samples also reflects the absorption properties of the photocatalysts for visible light. The inset of figure 4(a) illustrates that P25 and B-TiO_2 present as white and black in appearance, respectively, evidence that only B-TiO_2 is capable of effectively absorbing visible light. The visible light absorption feature of B-TiO_2 mainly originates from its structural modifications, such as large amounts of stable oxygen vacancies/Ti^{3+} dopants [12]. In this study, the optical absorption of the photocatalysts is important for the toluene removal in the PPS. Since the DBD can emit light within the range of 300–800 nm (see figure 2(d)), the PPS (B-TiO_2) would utilize light more efficiently than the PPS (P25) to drive the plasma photocatalytic reactions, favoring the mineralization of toluene. The stability of B-TiO_2 is also evaluated by comparing its UV–vis DRS before and after toluene removal. The used B-TiO_2 presents with a slightly different color in comparison with the fresh B-TiO_2, but strong absorption for visible light can still be observed for the used B-TiO_2, even after the cycled toluene removal reaction (figure 4(a)). This suggests a relatively good stability of B-TiO_2 in the toluene removal process. Here, the difference between fresh and used B-TiO_2 is probably caused by the discharge or adsorption of organic compounds on the photocatalyst surface. Note that this change occurs at the beginning of the toluene removal reaction, since B-TiO_2 obtained from the cycled reaction (30 h) possesses similar physical properties to that used in the 1 h continuous reaction according to our results.

PL spectra of the photocatalysts were obtained to measure the recombination of photo-generated electron–hole pairs. In figure 4(b), the emission peak at 410 nm originates from the band gap transition of anatase, peaks at 451 nm and 468 nm are ascribed to band edge free excitons and peaks at 482 nm and 492 nm are related to bound excitons. Although the fresh P25 and B-TiO_2 as well as used B-TiO_2 possess similar PL spectra shapes, they appear to have distinct PL intensity. The similar PL intensity of the fresh and used B-TiO_2 suggests excellent stability of B-TiO_2 in the plasma photocatalytic process, which is consistent with the XRD, Raman spectra and UV–vis DRS results. However, the distinct PL intensity between P25 and B-TiO_2 reflects different lifetimes of photo-generated electron–hole pairs for these photocatalysts. The strong intensity of the PL peaks of P25 implies its fast recombination rate of electron–hole pairs, which limits the photo-generated electrons and holes from participating in the plasma photocatalytic reactions. In contrast, the greatly reduced PL intensity for B-TiO_2 indicates the suppressed recombination of electrons and holes over the B-TiO_2 surface. This suggests that, compared with P25, B-TiO_2 in the PPS not only efficiently absorbs light emitted from the discharge to generate electron–hole pairs but it also endows electrons and holes with long lifetimes to effectively induce plasma photocatalytic removal of toluene. Apparently, an excellent performance of the PPS (B-TiO_2) in toluene removal can be expected according to the above analysis on optical properties of photocatalysts.

3.3. Toluene removal in PPS

In figure 5, the performances of the DBD alone, PPS (P25) and PPS (B-TiO_2) in toluene removal are displayed with the purpose of validating the advantages of the PPS (B-TiO_2). For comparison, the effect of light intensity on toluene removal over the photocatalysts was also evaluated. Figures 5(a) and (b) show that the PPS can present a better performance than the DBD alone at the same SEI. For example, at an SEI of

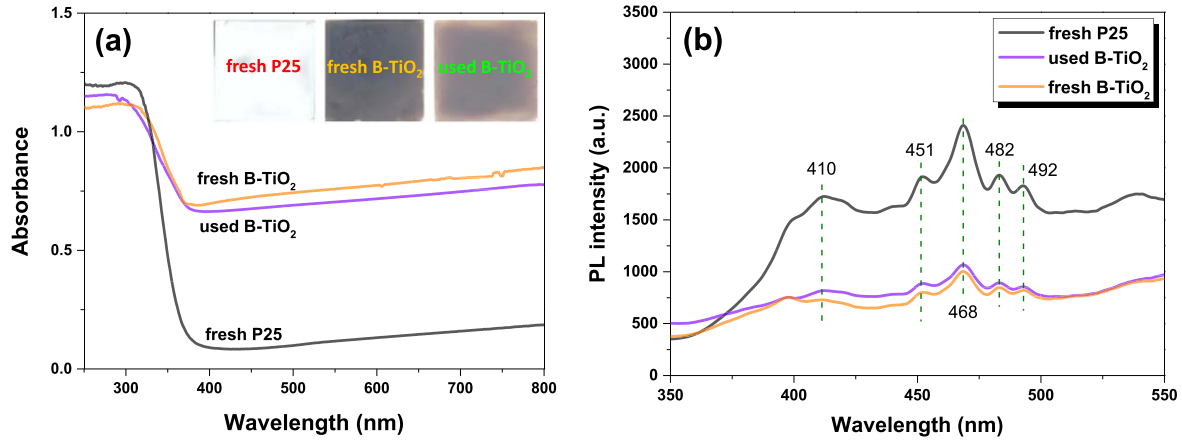

Figure 4. (a) UV–vis DRS and (b) PL spectra of the fresh and used photocatalysts. Inset of (a): photographs of the photocatalysts. The used B-TiO_2 was obtained after the cycled toluene removal reaction at an SEI of 1500 J · l^{-1}; two cycles were respectively performed for 15 h with an interval of 9 h.

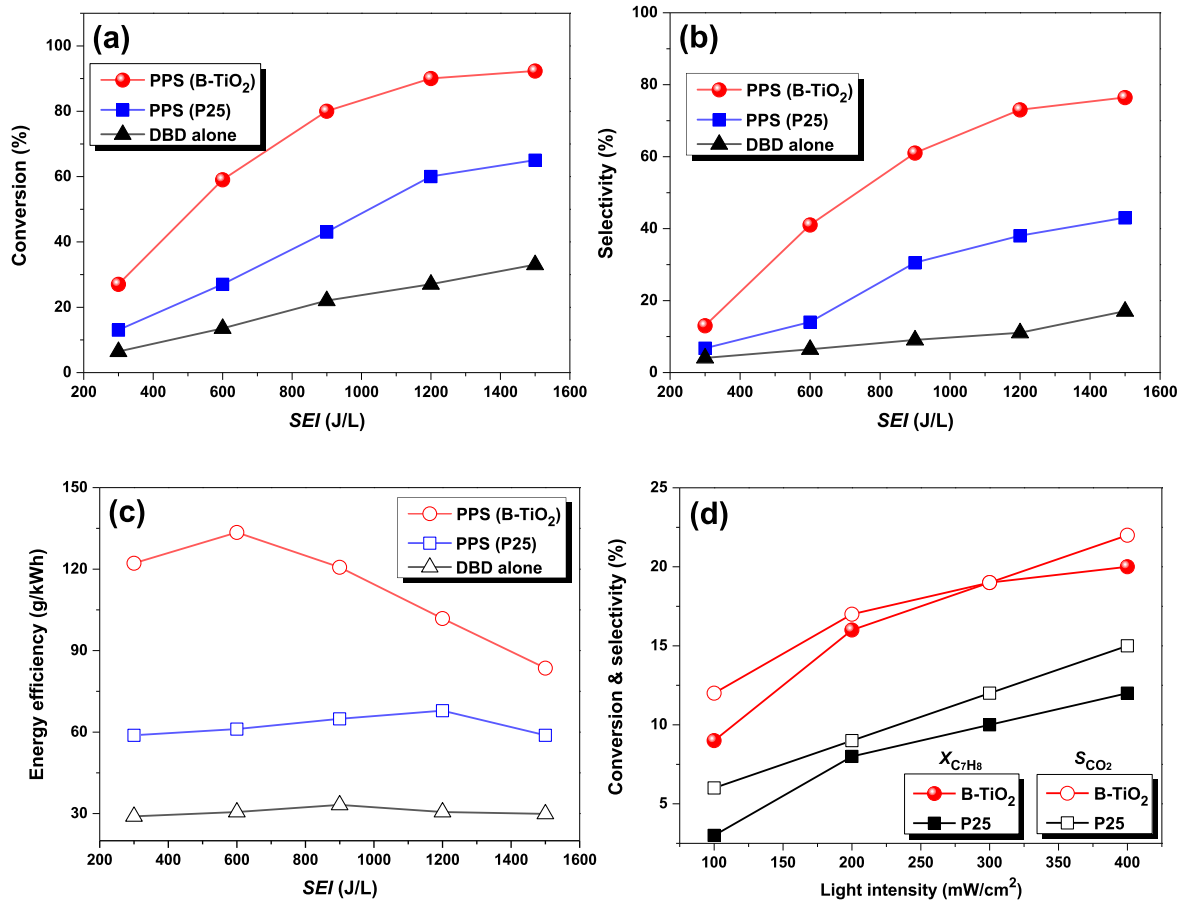

Figure 5. The effect of SEI on (a) $X_{C_7H_8}$, (b) S_{CO_2}, and (c) EE in different systems, and (d) the effect of light intensity on the performance of photocatalysts in toluene removal.

1200 J · l^{-1}, the DBD alone only obtains $X_{C_7H_8}$ of 27% and S_{CO_2} of 11%, but the PPS (P25) and PPS (B-TiO_2) can achieve much higher $X_{C_7H_8}$ (59% and 90%) and S_{CO_2} (38% and 73%). This not only demonstrates that the presence of photocatalysts in the discharge facilitates the mineralization of toluene, but also indicates that the performance of the PPS strongly depends on the properties of the photocatalysts. As expected, owing to its superior performance in toluene removal, the PPS (B-TiO_2) can achieve the highest EE of 133.5 g kWh^{-1} (SEI = 600 J · l^{-1}), which is much higher than those of the PPS (P25) and DBD alone (figure 5(c)). Interestingly, the highest EE of the PPS (B-TiO_2) is achieved at an SEI of 600 J · l^{-1}, whereas the PPS (P25) and DBD alone obtain the optimum values at an SEI of 1200 J · l^{-1}.

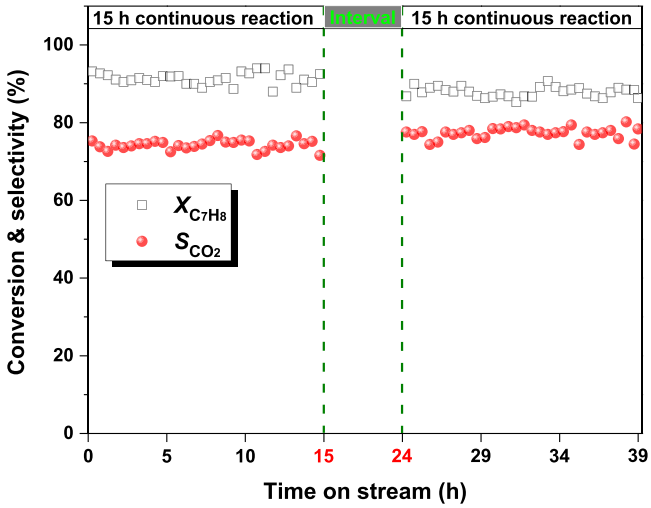

Figure 6. Stability of the PPS (B-TiO_2) in the cycled toluene removal process at an SEI of 1500 J · l^{-1}.

This is because the PPS (B-TiO_2) possesses high $X_{C_7H_8}$ at a relatively low SEI, and thus a further increase in SEI would lead to increased energy waste during toluene removal. Figure 5(d) illustrates the performance of photocatalysts in toluene removal under UV-visible light irradiation. For P25 and B-TiO_2, both $X_{C_7H_8}$ and S_{CO_2} present an increase with the increase in light intensity. Owing to its stronger absorption for visible light (figure 4(a)), B-TiO_2 exhibits a better performance than P25 in the photocatalytic removal of toluene. At a light intensity of 400 mW cm^{-2}, $X_{C_7H_8}$ and S_{CO_2} for B-TiO_2 are, respectively, 20% and 22%, which are higher than those of P25 (12% and 15%). Apparently, compared with PPS, the photocatalytic system shows a much lower performance in toluene oxidation because of the high chemical stability of toluene molecules. This also suggests a strong synergetic effect between the DBD and photocatalysts, especially for the PPS (B-TiO_2). For example, at an SEI of 1500 J · l^{-1}, the DBD alone only obtains $X_{C_7H_8}$ of 33% and a relatively weak light intensity, but the combination of DBD and B-TiO_2 makes $X_{C_7H_8}$ significantly increase to 92%. According to the results in section 3.2, this strong synergetic effect might lie in the fact that B-TiO_2 located in the discharge region provides a high concentration of oxygen vacancies for accelerating surface reactions, and efficiently absorbs UV-visible light emitted from the discharge to drive plasma photocatalytic reactions. Meanwhile, the effective activation of toluene in plasma plays a critical role in accelerating surface reactions over photocatalysts under the irradiation of light. In addition, compared with the DBD alone, a much higher discharge power at the same P_{in} also contributes to the enhanced performance in toluene removal.

As another important factor for evaluating the performance of the PPS in toluene removal, stability of the PPS (B-TiO_2) during a cycled toluene removal process was also investigated. As shown in figure 6, the cycled toluene removal reaction was performed at an SEI of 1500 J · l^{-1}, and the two cycles were continuously conducted for 15 h with an interval of 9 h. Obviously relatively stable $X_{C_7H_8}$ and S_{CO_2} are observed from figure 6, suggesting that the PPS (B-TiO_2) possesses good stability in the toluene removal. The durability of the PPS (B-TiO_2) should be attributed to the excellent stability of B-TiO_2, which has been discussed in section 3.2. The results shown in figures 5 and 6, taken together, confirm that the PPS (B-TiO_2) exhibits a superior performance in toluene removal.

3.4. Product analysis and mechanism of toluene removal

For the discharge in air, the formation of secondary pollutants such as ozone (O_3) and nitrogen oxides (NO_x) is normally inevitable. Since S_{CO_2} is less than 100%, organic intermediates also exist in the plasma photocatalytic process. Analyzing the distribution of gaseous products as well as the intermediates can provide more information for unravelling the mechanism of toluene removal. As a result, we used FT-IR and an O_3 analyzer to online monitor the gaseous products during the toluene removal process. Also, a mass spectrometer (MS) was used to further identify the organic intermediates formed in the PPS. In figure 7(a), the FT-IR spectra of the DBD alone and PPS (B-TiO_2) are compared. The formation of O_3 (1057 and 2120 cm^{-1}), N_2O (2237 cm^{-1}) and N_2O_5 (895, 1310, 1712 and 3550 cm^{-1}) can be clearly observed because of the discharge in air [24, 25]. The intensities of the IR bands for O_3 and NO_x are reduced when B-TiO_2 is placed into the discharge region, indicating that the exhaust of toxic by-products during toluene removal is effectively alleviated. In figure 7(b), the secondary pollutants of O_3, N_2O, NO_2 and N_2O_5 generated in these two systems are compared. Obviously, the PPS shows a decrease in the generation of O_3 and NO_x compared to the DBD alone, and the PPS (B-TiO_2) exhibits the lowest production of O_3 (1.1 g m^{-3}) and NO_x at the same SEI of 1500 J · l^{-1}. These results suggest that the secondary pollution originating from air discharge could be remarkably suppressed by applying the PPS (B-TiO_2). The secondary pollutants are closely related to the excited O atoms generated in the discharge [26, 27], which suggests that the accelerated plasma photocatalytic reactions between reactive organic intermediates and excited O atoms over B-TiO_2 could effectively suppress the formation of excited O atoms, and thus O_3 and NO_x. It is worth noting that the concentrations of O_3 and NO_x are still higher than the limitation concentration. Thus, a further decrease in the concentration of O_3 and NO_x is required in practical applications. According to our results, modulating the discharge atmosphere (such as increasing humidity) or constructing composite photocatalysts (such as the hybrid between TiO_2 and MnO_x) could greatly suppress the formation of O_3 and NO_x, which might be promising approaches for tackling the environmental effect of the PPS in future studies.

Figure 7(a) also shows that IR bands of CO_2 (2360 cm^{-1}), CO (2180 cm^{-1}), formic acid (1124 cm^{-1}) and benzaldehyde (1735 cm^{-1}) can be detected for both the DBD alone and PPS (B-TiO_2) due to the oxidation of toluene [26, 28]. The organic intermediate species are further confirmed by MS measurement. As shown in figures 7(c) and (d), formic acid (m/z = 45 and 46) and benzaldehyde (m/z = 77 and 105) are identified by MS. In addition, benzoic acid (m/z = 77, 105 and 122) and

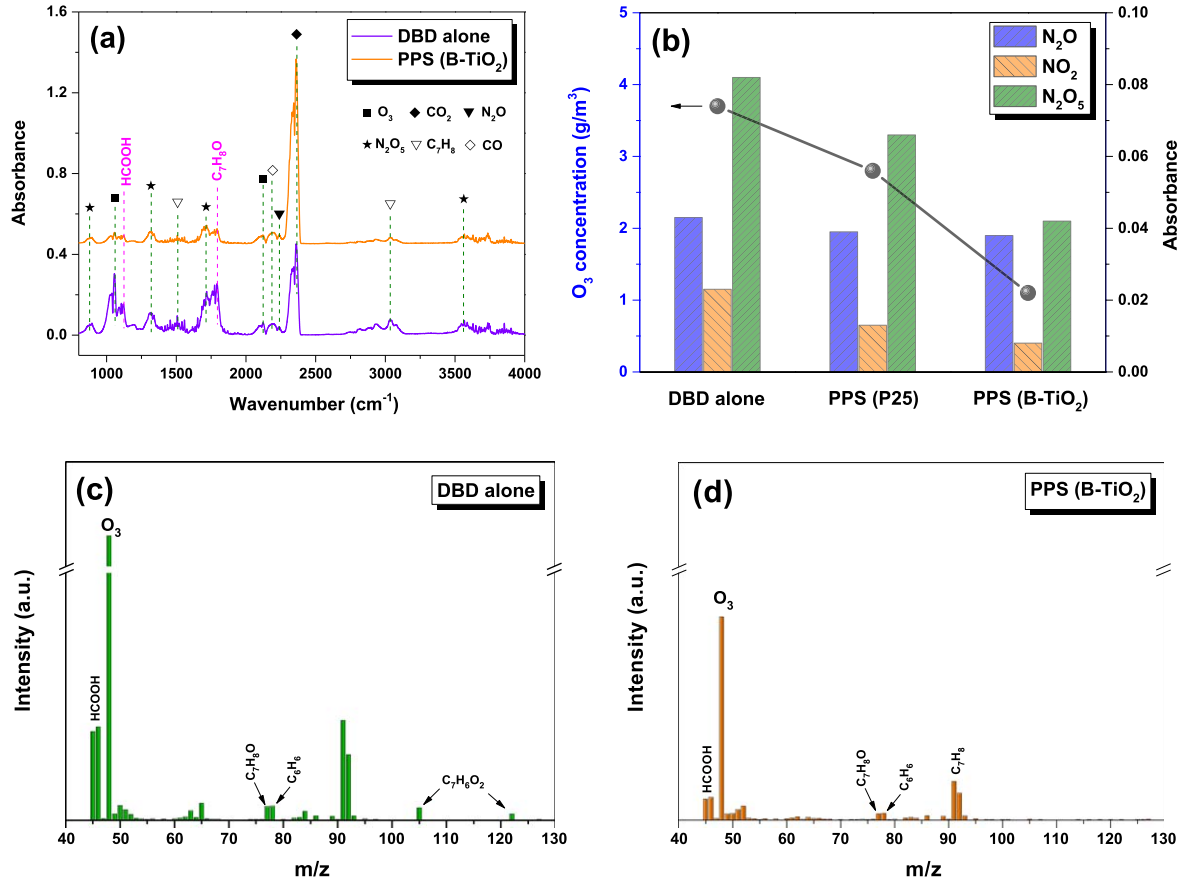

Figure 7. (a) FT-IR spectra of the gaseous products from the DBD alone and PPS (B-TiO_2), (b) O_3 concentration and IR peak intensity (absorbance) of formed NO_x for different systems and MS spectra of the effluent from (c) DBD alone and (d) PPS (B-TiO_2). Data were obtained at 30 min discharge time and an SEI of 1500 $J \cdot l^{-1}$.

benzene ($m/z = 77$ and 78) are also identified by MS for the DBD alone (figure 7(c)). These organic intermediates are generated from partial oxidation of toluene and could be further oxidized to CO_2 and H_2O. Moreover, the gaseous products as well as organic intermediates show differences in their intensities for the DBD alone and PPS (B-TiO_2). According to figure 7(a), the PPS (B-TiO_2) possesses a stronger peak of CO_2 but weaker bands of benzaldehyde and formic acid compared with the DBD alone, because the presence of B-TiO_2 in the discharge benefits the deep oxidation of intermediates, such as benzaldehyde, formic acid, into CO_2. This point is also supported by the MS results. Compared with the DBD alone, the MS signal intensity of formic acid, benzaldehyde and benzene in the PPS (B-TiO_2) is obviously reduced. Further, the benzoic acid signal disappears in the PPS (B-TiO_2) due to the accelerated rate of the oxidation reaction.

The DBD alone attains a relatively poor $X_{C_7H_8}$ and S_{CO_2} because the toluene removal in this system only depends on the homogeneous reaction in the gas phase [29]. Large numbers of active species, such as electrons, ions and radicals, formed in the DBD can induce toluene removal (e.g. equations (6) and (7)) at low temperatures. Owing to the high energy of electrons, the aromatic ring of toluene can be opened. However, the homogeneous gas reactions in plasma suffer from low reaction rates, limiting the performance of the DBD alone in toluene removal.

$$C_6H_5CH_3 + e \rightarrow C_6H_5CH_2 + H + e \quad (6)$$

$$C_6H_5CH_2 + O \rightarrow C_6H_5CH_2O. \quad (7)$$

For toluene removal in the PPS (B-TiO_2), the discharge still induces homogeneous gas reactions, but the integration of the DBD and B-TiO_2 makes surface photocatalytic reactions occurring on B-TiO_2 dominate the performance of the PPS (B-TiO_2). In fact, the superior performance of the PPS (B-TiO_2) in toluene removal should be attributed to the strong synergetic effect between plasma and B-TiO_2. Firstly, the DBD can not only activate toluene molecules and provide numbers of active species for surface photocatalytic reactions, but it can also emit UV-visible light to drive the oxidation reactions over B-TiO_2. Secondly, integrating B-TiO_2 with the DBD makes the discharge transform from the filamentary mode into a relatively uniform mode and leads to the increased discharge power. This benefits the generation of active species, and also alleviates the production of NO_x due to the suppressed formation of NO under undermined current pulses [24, 26]. Lastly, and most significantly, B-TiO_2 possesses abundant surface oxygen vacancies and strong absorption ability for UV-visible light, which makes the PPS (B-TiO_2) utilize light emitted from the discharge to efficiently catalyze surface reactions between active species, such as O,

·OH, N_2^+, O_3 and O_2^-, and absorbed toluene molecules, thus enabling the acceleration of deep oxidation of organic intermediates to CO_2. These enhanced photocatalytic reactions between organic intermediates and oxidative species in the PPS (B-TiO_2) would contribute to the suppression of the concentration of O_3 and NO_x, and thus high stability of the PPS (B-TiO_2) because the accumulation of these species on the active sites of B-TiO_2 is suppressed.

4. Conclusion

A PPS constructed by integrating a B-TiO_2 photocatalyst with a DBD exhibited superior activity and CO_2 selectivity, as well as stability for removing toluene from air. The strong synergetic effect between B-TiO_2 and plasma, and suppressed formation of secondary pollutants of O_3 and NO_x were achieved for the PPS (B-TiO_2), because B-TiO_2 not only possessed a high concentration of oxygen vacancies but it also exhibited efficient absorption for UV-visible light emitted from the discharge. The presence of B-TiO_2 in the discharge region also led to the increased discharge efficiency of the DBD, thus contributing to enhanced oxidation of toluene into CO_2. The PPS (B-TiO_2) in this study simultaneously tackled the problems of relatively poor activity and stability of the conventional PPS, providing a promising approach for the abatement of refractory VOCs from air.

Acknowledgments

This work is supported by National Natural Science Foundation of China (No. 21808024) and Fundamental Research Funds for the Central Universities (DMU 3132018175). B Zhu and Y M Zhu thank Prof. Fuqiang Huang, from Shanghai Institute of Ceramics, for providing the photocatalysts in this work.

References

[1] Van Durme J *et al* 2008 *Appl. Catal. B: Environ.* **78** 324
[2] Chen H L *et al* 2008 *Appl. Catal. B: Environ.* **85** 1
[3] Tu X and Whitehead J C 2012 *Appl. Catal. B: Environ.* **125** 439
[4] Wu J L *et al* 2013 *Plasma Chem. Plasma Process.* **33** 1073
[5] Wang J T *et al* 2016 *Plasma Sci. Technol.* **18** 370
[6] Chen H L *et al* 2009 *Environ. Sci. Technol.* **43** 2216
[7] Huang H B *et al* 2007 *Plasma Chem. Plasma Process.* **27** 577
[8] Ochiai T *et al* 2012 *Chem. Eng. J.* **209** 313
[9] Wang H J and Chen X Y 2011 *J. Hazard. Mater.* **186** 1888
[10] Deng X Q *et al* 2016 *Appl. Catal. B: Environ.* **188** 48
[11] Sun Z G *et al* 2018 *Plasma Process. Polym.* **15** 1800095
[12] Liu X Y *et al* 2016 *Adv. Energy Mater.* **6** 1600452
[13] Yang C Y *et al* 2013 *J. Am. Chem. Soc.* **135** 17831
[14] Li X S *et al* 2019 *Catal. Today* (https://doi.org/10.1016/j.cattod.2019.03.033)
[15] Sun Z G *et al* 2019 *J. Catal.* **375** 380
[16] Deng X Q *et al* 2017 *Catal. Today* **281** 630
[17] Fan X *et al* 2009 *Chemosphere* **75** 1301
[18] Kogelschatz U 2002 *IEEE Trans. Plasma Sci.* **30** 1400
[19] Ráhel J and Sherman D M 2005 *J. Phys. D: Appl. Phys.* **38** 547
[20] Li M *et al* 2018 *Plasma Chem. Plasma Process.* **38** 1063
[21] Li M *et al* 2019 *Appl. Phys. Lett.* **114** 114102
[22] Wang Z *et al* 2013 *Energy Environ. Sci.* **6** 3007
[23] Wang Z *et al* 2013 *Adv. Funct. Mater.* **23** 5444
[24] Zhu B *et al* 2017 *Top. Catal.* **60** 914
[25] Zhu B *et al* 2015 *Appl. Catal. B: Environ.* **179** 69
[26] Zhu B *et al* 2018 *Plasma Process. Polym.* **15** 1700215
[27] Zhao D Z *et al* 2011 *Chem. Eng. Sci.* **66** 3922
[28] Fan H Y *et al* 2012 *Appl. Catal. B: Environ.* **119–120** 49
[29] Xu X X *et al* 2016 *Chem. Eng. J.* **283** 276